

# An All-Metal Micro-Relay With Bulk Foil Pt–Rh Contacts for High-Power RF Applications

Fatih M. Ozkeskin, *Member, IEEE*, Sangjo Choi, *Student Member, IEEE*,  
Kamal Sarabandi, *Fellow, IEEE*, and Yogesh B. Gianchandani, *Fellow, IEEE*

**Abstract**—This paper describes the performance of stainless-steel micro-relays, with platinum–rhodium metal foil contact elements, in handling high-power RF signals. The electrical and thermal responses are described for electrostatically actuated three-terminal micro-relays that are directly assembled on printed circuit boards. The preliminary designs have footprints of 6.4 mm<sup>2</sup>. Fabricated relays have 90-V turn-on (pull-down) voltage. The down-state insertion loss and up-state isolation were better than 0.2 and 25 dB over the band of dc–5 GHz, respectively. The devices can accommodate incident RF power up to 18.5 W at 3 GHz when cooled by forced air from a mini-fan.

**Index Terms**—Cantilever, heat sink, micro-relay, platinum–rhodium (Pt–Rh), RF switch.

## I. INTRODUCTION

MICRO-RELAYS are widely used in signal switching for applications in the aerospace sector, RF communications, and portable electronics. There has been extensive research on the miniaturization and integration of micro-relays as a result of the recent developments in the microfabrication techniques [1]–[5]. Compared to solid-state counterparts, the micromechanical RF switches hold the promise of advantages including high linearity, low loss, and low power consumption [6]–[11]. However, the focus has been on devices that handle relatively low levels of RF power, i.e. below 100 mW. High RF power handling in micro-relays is needed for satellite transmitters and earth-based communications stations [12], [13].

This paper is directed at options for direct contact micro-relays that can accommodate power levels exceeding 1 W. Challenges include not only self-actuation in the up-state, but also dominant failure mechanisms such as metal softening and micro-welding in the down-state. Contact failure mechanisms

that define the power-handling capability of the ohmic-contact micro-relays are related to the nature of the contact metals [14], [15].

Most of the past efforts in high-power RF micro-relays have focused on surface micromachined contact materials for increased power handling [16], [17]. Surface micromachining techniques only allow the use of metals that can be sputtered or electroplated. Micro-relays micromachined from bulk foils can utilize metal alloys, and take advantage of the properties such as high hardness and high melting point, and thereby accommodate high RF power.

Platinum–rhodium (Pt–Rh) is a mechanically robust and chemically inert metal alloy that is used in very high-quality crucibles. Pt–Rh alloy with 20% Rh content has higher hardness and higher melting point than pure platinum [18], [19]. Platinum group contact metals are also known to considerably reduce stiction [20], [21]. These properties make Pt–Rh an attractive candidate for high-power RF micro-relays; it is expected to be resistant to softening and micro-welding at elevated temperatures that may rise during high-power signal transmission.

This paper describes the performance of electrostatically actuated three-terminal micro-relays that utilize a cantilever, a contact bridge, and an on-device heat sink.<sup>1</sup> Section II describes the micro-relay design, and Section III details the fabrication and assembly processes for the device. Experimental evaluation is presented in Section IV. These include dc, small-signal, and high-power RF characterization, thermal performance, and lifetime test for the device. Section V provides discussion and conclusions.

## II. DESIGN

The micro-relay has a three-terminal structure (Fig. 1). The design has a footprint of 6.4 mm<sup>2</sup> and it is composed of vertically stacked components directly located and assembled on a printed circuit board (PCB). The PCB uses a Rogers 4003 substrate with Cu–Ni–Au traces (75-, 4-, and 0.15- $\mu$ m thicknesses, respectively) for reduced loss at microwave frequencies. The PCB traces have four regions. The first region includes two transmission line segments with 50- $\Omega$  characteristic impedance and provides input and output paths for the RF signal. At the end of each line, the terminals accommodate contact regions (200  $\mu$ m  $\times$  200  $\mu$ m each). The second region includes the dc ground. Two types of vias are defined on the dc ground: isolated vias provide the locations for anchoring and assembly purposes, and plated vias short dc and RF grounds. The third region includes an L-shaped electrode for the placement of a dc-blocking

<sup>1</sup>Portions of this work have been reported in conference abstract form in [22].

Manuscript received August 01, 2011; revised March 02, 2012; accepted March 08, 2012. Date of publication April 26, 2012; date of current version May 25, 2012. This work was supported in part by the Microsystems Technology Office (MTO), Defense Advanced Research Projects Agency (DARPA) under Contract W31P4Q-09-1-0009.

F. M. Ozkeskin was with the Mechanical Engineering Department, The University of Michigan at Ann Arbor, Ann Arbor, MI 48109 USA. He is now with Applied Materials, Santa Clara, CA 95054-3299 USA (e-mail: ozkeskin@umich.edu).

S. Choi and K. Sarabandi are with the Radiation Laboratory, Electrical Engineering and Computer Science Department, The University of Michigan at Ann Arbor, Ann Arbor, MI 48109 USA (e-mail: sangjo@umich.edu; saraband@eecs.umich.edu).

Y. Gianchandani is with the Electrical Engineering Department and the Mechanical Engineering Department, The University of Michigan at Ann Arbor, Ann Arbor, MI 48109 USA (e-mail: yogesh@umich.edu).

Color versions of one or more of the figures in this paper are available online at <http://ieeexplore.ieee.org>.

Digital Object Identifier 10.1109/TMTT.2012.2192744

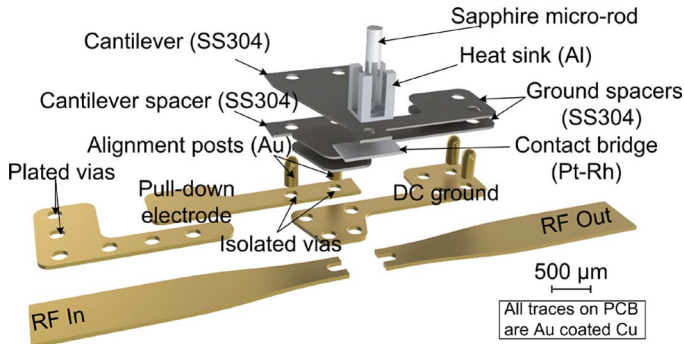


Fig. 1. Exploded view of the three-terminal micro-relay. Four regions of the PCB are shown. Cantilever and ground spacers, both from stainless steel, are placed to elevate the cantilever above the signal line to define the actuation and the contact gaps. Gold posts align and hold the spacers and the cantilever over the gold-coated copper traces on the PCB. Cantilever pushes the Pt–Rh contact bridge, located at the distal end, via a micro-rod, which couples both components. An Al heat sink is integrated atop the point of contact. Device footprint (as defined by the footprint of the cantilever) is  $6.4 \text{ mm}^2$ .

capacitor. It also acts as a shield to further reduce the RF signal coupling from the transmission line. The fourth region includes the pull-down electrode; it is used to electrostatically actuate the cantilever. The PCB design is obtained through iterative optimization and sensitivity studies to provide the desired switching RF performance. The simulations are described toward the end of this section.

The stainless-steel cantilever is positioned orthogonally with respect to the transmission line and suspended above a break. It defines the device footprint ( $2000 \mu\text{m} \times 3200 \mu\text{m}$ , including anchor;  $2700\text{-}\mu\text{m}$  suspended length;  $50\text{-}\mu\text{m}$  thick). The cantilever is elevated above the pull-down electrode on the PCB by a cantilever spacer ( $2000 \mu\text{m} \times 400 \mu\text{m} \times 110 \mu\text{m}$ ). Two identical ground spacers ( $4000 \mu\text{m} \times 2350 \mu\text{m} \times 50 \mu\text{m}$  each) are stacked on the ground electrode. For electrostatic actuation, an interelectrode gap of  $10 \mu\text{m}$  is maintained between the bottom surface of the cantilever and the top surface of the ground spacer stack. The actuation electrode size is defined by the trapezoidal overlap area between ground spacers and the cantilever ( $1.8 \text{ mm}^2$ ). A pair of gold alignment posts ( $400\text{-}\mu\text{m}$  height,  $300\text{-}\mu\text{m}$  diameter each) perforates and anchors the cantilever spacer and the cantilever to the pull-down electrode and the PCB substrate through tightly fitting into the isolated vias. Another pair of alignment posts with same diameter similarly anchors ground spacers to the ground electrode.

At the distal end of the cantilever is a multilevel vertically stacked structure. A Pt–Rh contact bridge ( $600 \mu\text{m} \times 1000 \mu\text{m} \times 30 \mu\text{m}$ ), provides an ohmic contact between two open ends of the microstrip underneath. A thermally conductive sapphire micro-rod ( $700\text{-}\mu\text{m}$  height,  $250\text{-}\mu\text{m}$  diameter,  $50\text{-W} \cdot \text{K}^{-1} \cdot \text{m}^{-1}$  thermal conductivity, Meller Optics Inc.) is used to mechanically couple the contact bridge with the cantilever and electrically separate them. It also performs as a thermal conductor to take the heat away from the contact regions. The micro-rod rests on a  $5\text{-}\mu\text{m}$ -deep blind hole at the center of the contact bridge and centers the stacked components by perforating the concentric holes on them. The gap between the cantilever and the contact bridge is designed so that the latter stands  $12 \mu\text{m}$  above the transmission line.

A micromachined aluminum heat sink ( $600 \mu\text{m} \times 600 \mu\text{m} \times 1000 \mu\text{m}$ ) with four fins (each  $150 \mu\text{m} \times 150 \mu\text{m}$  and  $950\text{-}\mu\text{m}$  tall) is used to dissipate local contact heating through active cooling when combined with a commercially available mini-fan (Sunon-UF3A3) placed  $1.5 \text{ mm}$  above the transmission line. The gap between the fins is defined to allow the location of the micro-rod. Heat-sink design follows the principles described in [23]. Two criteria were followed for designing the heat sink fins, which are: 1) heat loss limit should be larger than 1 and 2) fin efficiency should be larger than 0.75. The heat loss limit,  $h_l$ , is defined by

$$h_l = \frac{2k}{ht} \geq 1 \quad (1)$$

where  $k$  is the thermal conductivity of the sink material ( $\text{W} \cdot \text{K}^{-1} \cdot \text{m}^{-1}$ ),  $h$  is the heat transfer coefficient ( $\text{W}/\text{m}^2 \cdot \text{K}$ ) and  $t$  is the fin width (m). At room temperature ( $300 \text{ K}$ ), for air ambient and a fin width of  $150 \mu\text{m}$ , the heat loss limit is 4.91. Fin efficiency is defined by

$$\eta = \frac{\tanh(mL)}{mL} \geq 0.75 \quad m = \sqrt{\frac{2h}{kt}} \quad (2)$$

where  $L$  is the fin height. For a fin height of  $950 \mu\text{m}$ , the fin efficiency is 0.876.

Electrostatic modeling of the RF micro-relay was performed in the ANSYS Workbench finite-element analysis (FEA) environment. Fig. 2 shows the displacement and stress distribution. The model consisted only of the micro-relay and the transmission line. Other electrodes on the PCB were neglected. The “bonded contact” boundary conditions were used for touching surfaces. The “fixed geometry” boundary condition was applied around the alignment posts on the anchor points. For a  $12\text{-}\mu\text{m}$  vertical tip displacement, pull-down voltage was  $85 \text{ V}$ . The FEA results show that the displacement across the  $10\text{-}\mu\text{m}$  interelectrode gap over the ground electrode was approximately  $4 \mu\text{m}$  when the contact occurs, therefore pull-in was prevented. The stiffness of the entire micro-relay including the cantilever, heat sink, contact bridge, and micro-rod was  $142 \text{ N}/\text{m}$ . The contact force per contact region was  $0.36 \text{ mN}$  (with  $1.44 \text{ mN}$  evenly distributed over four contact regions) for an increased actuation voltage of  $130 \text{ V}$ . The switching time was  $16 \text{ ms}$ .

An estimate of the contact resistance is required for two reasons: for accurately modeling  $S$ -parameters in the High Frequency Structure Simulator (HFSS), and for use as a boundary condition in the thermal model to account for high-power joule heating. The contact resistance model is based on Holm’s plastic deformation theory [24].

The model suggests that

$$F = A_C H n \quad (3)$$

where  $F$  is the contact force,  $A_C$  is the actual mechanical contact area of overlapping contact asperities between touching surfaces,  $H$  is the contact metal hardness, and  $n$  is an empirical factor, which depends on material and approaches 1 for clean surfaces. Incorporating contact radius into this model gives

$$\alpha_H = \sqrt{\frac{F}{H n \pi}} \quad (4)$$

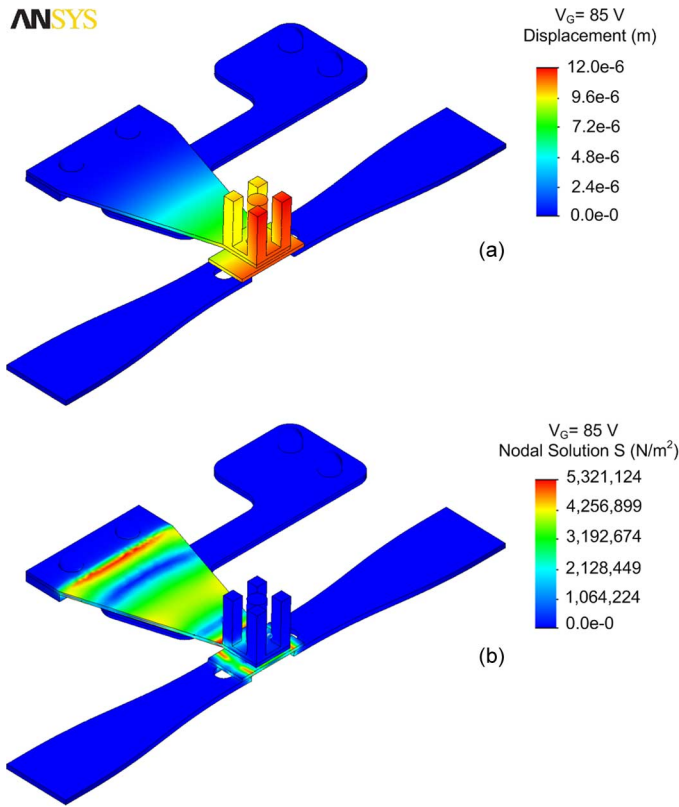


Fig. 2. Electrostatic FEA for RF micro-relay. (a) Tip displacement was  $12\ \mu\text{m}$  as a result of 85-V pull-down voltage. (b) Von Mises stress distribution after the contact. All four contact points had the same stress. Simulated total contact force and actuation time were 1.44 mN (evenly distributed over four contact regions) and 16 ms for 130-V actuation voltage, respectively.

where  $\alpha_H$  is the radius of Holm's contact spot ( $\alpha$ -spot) representing a cluster of multiple small contact spots. Contact radius  $\alpha_H$  can be used to estimate the Maxwell spreading resistance between two contacting surfaces assuming that the contact radius is much larger than the electron mean free path length of contacting materials. This spreading resistance is also known as constriction resistance  $R_C$

$$R_C = \frac{\rho_1 + \rho_2}{4\alpha_H}. \quad (5)$$

Here,  $\rho_1$  and  $\rho_2$  are the electrical resistivities of the contacting metals [25]. Referring to [26], it can be assumed that the contact pressures on a contacting pair of asperities are equal to the flow pressure of the softer of the two contacting materials. However, it is worth noting that in a multilayered contact design, the effective hardness is primarily determined by the thicker bottom layer material. Determining an exact value for the hardness in the multilayered Cu–Ni–Au patterns used for the PCB traces is nontrivial. Since the thickness of the Ni layer ( $4\ \mu\text{m}$ ) is sufficiently larger than the thickness of the Au ( $0.15\ \mu\text{m}$ ), the effective hardness was chosen as that of Ni. Using (4) and (5), a total series contact resistance of  $1.09\ \Omega$  was analytically estimated for the RF micro-relay, assuming a contact hardness of 6 GPa—the approximate Meyer hardness of Ni, estimated total resistivity of  $30\ \mu\Omega \cdot \text{cm}$  for Pt–Rh/Cu–Ni–Au stacked contacts, and 0.36-mN contact force per contact region, as noted above. The resulting

radius for Holm's  $\alpha$ -spot, i.e., single contact spot representing a cluster of multiple small contact spots was 137 nm. For experimental validation, a Pt–Rh beam with the same dimensions as in the proposed design was pressed against the open signal lines on the PCB. A precision force gauge (Aurora Scientific, Model 403A), which was mounted on a motorized  $x$ – $y$ – $z$  stage, supplied the contact force. The force was applied in  $80\text{-}\mu\text{N}$  increments, up to 1.44 mN, over a 1-mm contact diameter. Contact resistance was measured using a four-wire technique with a 5-mA test current. The total series resistance was  $1.34\ \Omega$  for 1.44-mN total contact force. The empirically estimated radius of the  $\alpha$ -spot was 111 nm.

The transmission line and the dc electrodes were refined to reduce the RF coupling and the fringing, which commonly appear in high-frequency RF devices. Geometric optimization involved iterative RF full-wave simulations in HFSS. The simulations were performed for the micro-relay in both the down- and up-state. In the down-state, the contact resistance of  $1.34\ \Omega$  was used as a lumped element. The electric field distribution at 10 GHz guided the geometric modifications depicted in three configurations (Figs. 3 and 4). In Configuration-1, the dc ground and the pull-down electrode had only isolated vias for anchoring the structural elements; hence, significant coupling was observed between the transmission line, the pull-down electrode, and the dc ground both in the up- and down-state. In Configuration-2, the dc ground electrode was shunted to the RF ground through the conductive plated vias. In addition, the contact pad for the pull-down electrode was flipped horizontally to face away from the input transmission line, and all the electrode corners were rounded to reduce the level of fringing fields. Although the coupling between the transmission line and the dc ground electrode was reduced significantly, the electric field was not completely suppressed on the pull-down electrode. Configuration-3 was the final layout geometry and included: 1) the L-shaped electrode, which acted as a shield to reduce the coupling from the input transmission line; 2) the fork-shaped open ends, which reduced the up-state capacitance and dissipation through the contact bridge; and 3) smooth variation of linewidth for reduced reflection. A 1-pF capacitor was chosen to short circuit the RF path on the pull-down electrode and acted as a dc block. The coupling was considerably suppressed both in the down- and up-states.

Fig. 5 shows the  $S$ -parameters for each configuration in the down- and up-state. In the down-state, Configuration-3 resulted in overall better insertion loss and return loss compared to the other configurations at higher frequencies. Similarly, in the up-state, Configuration-3 has return loss better than 0.4 dB at 10 GHz, whereas the isolation is best throughout the bandwidth.

Thermal modeling of the micro-relay involved the extraction of the electric field distribution at 3 GHz and 30 W of RF power. The contact resistance was included in the model. The solution was then imported into the ANSYS Multiphysics solver to serve as the boundary condition. These values were chosen due to the experimental limits. The thermal adhesive between micro-rod, cantilever and heat sink was modeled as a shell with a thermal conductivity of  $5\ \text{W/m} \cdot \text{K}$  following the specifications of a commercially available epoxy (Aavid Thermalloy). Contact temperature modeling considered two on-state times: 1 and

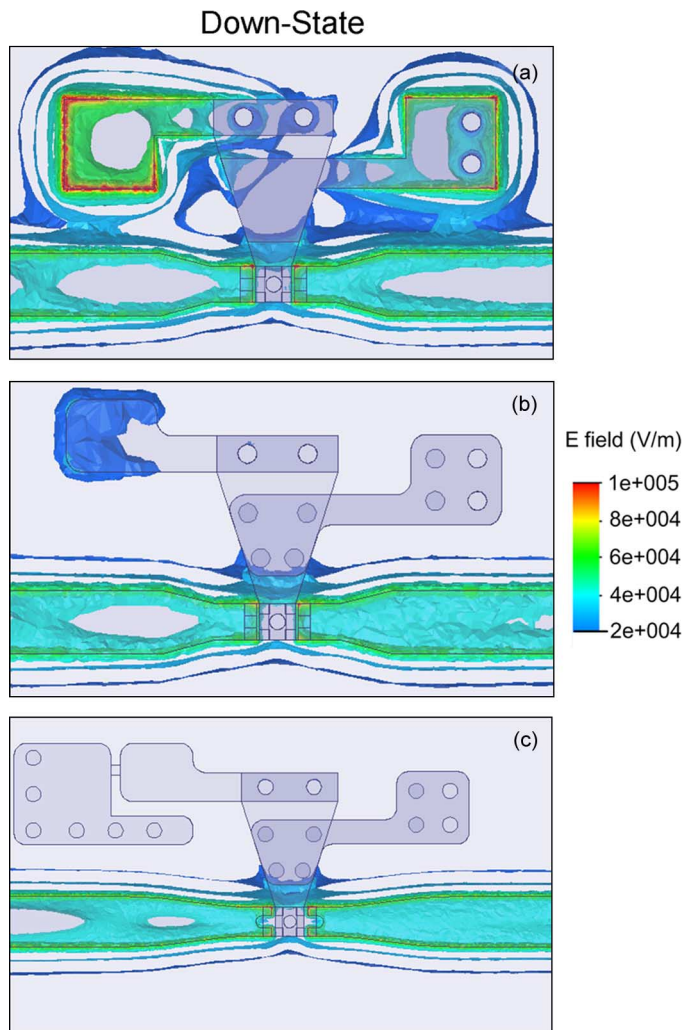


Fig. 3. Electric field distribution at 10 GHz for three configurations in the down-state. (a) In Configuration-1, the dc ground electrode had no plated vias. (b) In Configuration-2, the dc ground electrode had plated vias shunted to RF ground. In addition, the corners of the electrodes were rounded and the contact pad for the pull-down was flipped away from the transmission line. (c) In Configuration-3, the L-shaped electrode was placed next to the pull-down electrode and shunted to the RF ground through plated vias. A 1-pF dc-blocking capacitor was assumed. The transmission line was designed to have smooth variation of width. In addition, it had fork-shaped open ends to reduce the capacitance with the contact bridge and the dissipation through it. Configuration-3 provided an electric field distribution with minimized coupling to dc ground and pull-down electrode.

20 s. Forced cooling was assumed in the model; the manufacturer-specified upward air flow rate of 0.22 m/s was assumed to exist in an imaginary tube enclosing the contact bridge and heat sink (1.5-mm height, 1-mm diameter). Fig. 6 shows a temperature increase of approximately 185 K on contacts for 30 W of RF power that was continuously transmitted for 1 s in an unforced cooling setup. The simulation showed that forced cooling reduces the contact temperatures by approximately 25 K. Temperature rise times were 0.9 and 5.8 s for unforced and forced cooling cases, respectively.

### III. FABRICATION AND ASSEMBLY

Micro-electrodischarge machining ( $\mu$ EDM) is a lithography-compatible electrothermal machining technique, suitable

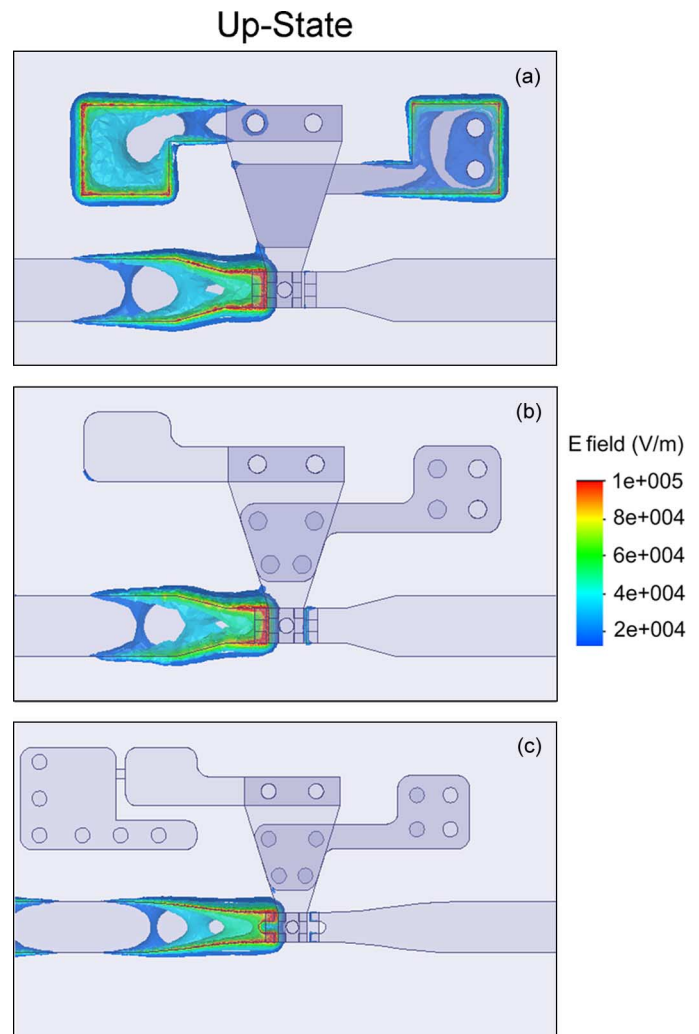


Fig. 4. Electric field distribution at 10 GHz for three configurations in the up-state. The geometries in (a)–(c) correspond to the geometries (a)–(c) in Fig. 3.

for metal alloy foil devices. Micromachining of features with sizes as small as 5  $\mu$ m can be achieved, both in serial mode (using a cylindrical wire-tip electrode), and in batch mode (using a lithographically patterned and electroplated chip as a “cookie-cutter”) [27].

For the micro-relay, the contact bridges were serially fabricated using  $\mu$ EDM in Pt–Rh (Alfa Aesar Corporation, 80:20 concentration, 99.99% purity) down to 30- $\mu$ m final thickness using 50- $\mu$ m-thick stock metal foils. The lowest available discharge energy of 24.5 nJ was used at contact bridges to ensure a smooth surface finish. Surface roughness on the bottom unmachined side of the contact bridges was measured using a Zygo NewView 5000 interferometer. Average roughness  $R_a$  was approximately 25 nm.

The heat sinks were also fabricated using  $\mu$ EDM from 1-mm-thick Al 3003 alloy foil (99% purity). The discharge energy was increased to 16.5  $\mu$ J for faster machining of the fins. A hole of 250- $\mu$ m diameter was machined at the base of the heat sink for the subsequent assembly of the micro-rod and the contact bridge.

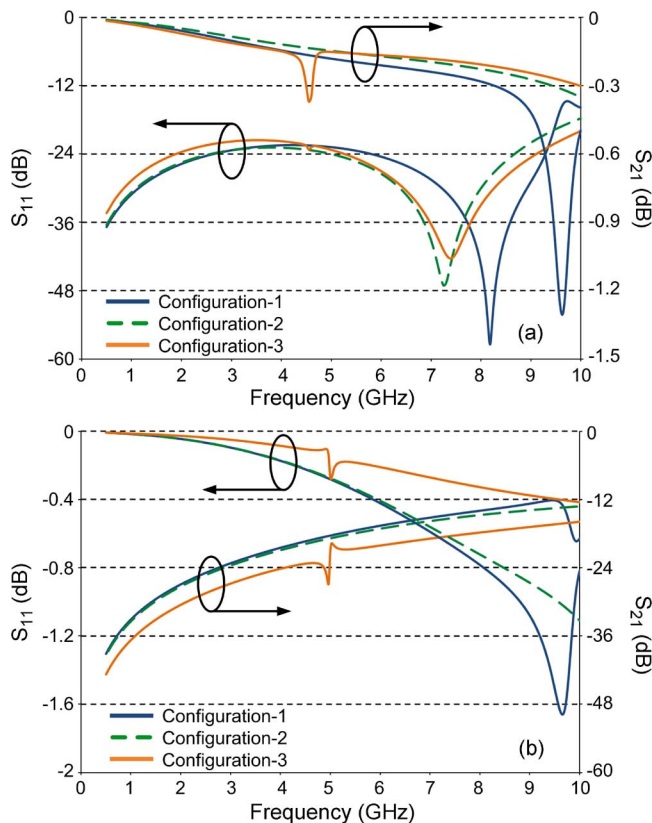


Fig. 5. Full-wave HFSS simulation results showing  $S$ -parameters for three configurations. (a) In the down-state, Configuration-3 provides the best insertion loss and return loss at higher frequencies. (b) In the up-state, Configuration-3 presents return loss better than 0.4 dB at 10 GHz. The isolation is also better than other configurations by about 4 dB over the bandwidth.

The cantilever spacer was also fabricated using  $\mu$ EDM down to 110- $\mu$ m thickness from 125- $\mu$ m-thick stainless-steel (SS304) stock foil. For each micro-relay, two perforations of 300- $\mu$ m diameter were positioned on the cantilever spacers to allocate the alignment posts for the attachment to the cantilever, and to the pull-down electrode below.

The cantilever and ground spacers were photochemically machined from 50- $\mu$ m-thick SS304 foils (Kemac Technology Inc.). Two perforations of 300- $\mu$ m diameter were located on the cantilever for the assembly over the cantilever spacer and the PCB, whereas another perforation of 250- $\mu$ m diameter was situated toward the tip of the cantilever for subsequent assembly of the contact bridge, micro-rod, and heat sink. Similarly, two perforations of 300- $\mu$ m diameter were positioned on the ground spacers for the attachment to the ground electrode.

500- $\mu$ m-thick Rogers 4003 was used as the substrate for the RF transmission line (Advanced Circuits Inc.). Cu traces provided the bias electrodes and the surface microstrip. In such PCBs, Ni was used as an adhesion layer on the Cu base, and an outer gold layer provided a low-resistivity electrical contact. Cu–Ni–Au metal tracing with the same thicknesses was used on the plated vias, whereas isolated vias were left unplated.

Alignment posts were fabricated using  $\mu$ EDM from 300- $\mu$ m-diameter gold wire, and tightly fitted into the isolated vias on the PCB [see Fig. 7(a)]. Conical wire tips facilitated the alignment and the insertion of the perforated components. The can-

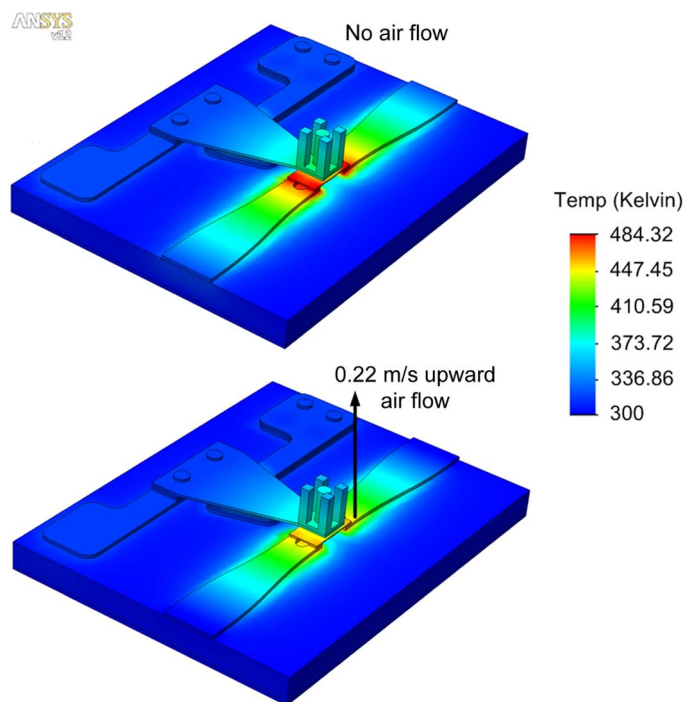


Fig. 6. Multiphysics electrothermal FEA results for 1 s into the on-state. The HFSS high-power electric field distribution was imported to ANSYS as a joule heating boundary condition. Contact area temperatures for: (a) unforced and (b) forced cooling (3-GHz 30-W incident RF power, 1.34- $\Omega$  modeled contact resistance, 300-K ambient temperature, 0.22-m/s upward flow).

tilever spacers and the ground spacers were assembled over the posts [see Fig. 7(b)] and fixed by applying an electrically conductive epoxy (Creative Materials, volume resistivity: 300  $\mu\Omega \cdot \text{cm}$ ). The assembly of the cantilever and heat sink followed this [see Fig. 7(c)]. The heat sink was attached onto the cantilever by aligning the perforation at its base to the one on the cantilever tip, and securing with high temperature epoxy (Cotronics Duralco 4703, 645-K maximum temperature). The flatness of the cantilever, as well as critical gap of 10  $\mu$ m, was maintained during the assembly process with the help of a high-resolution laser displacement sensor (Keyence LK-G32) raster scanning over the region and giving continuous feedback. The contact bridge was aligned and placed on the transmission line. The sapphire micro-rod was then tightly fitted into the overlapping perforations on the heat sink and cantilever. It rested on the blind hole at the center of the contact bridge, further aligning it for a precise contact. High-temperature epoxy was applied to fix the parts [see Fig. 7(d)].

A total of five devices were fabricated and assembled. The distribution of those devices is as follows: one device for dc on-state resistance characterization and hysteresis study; one device for small-signal characterization; two devices for high power testing and for thermal characterization; and one device for lifetime characterization.

#### IV. EXPERIMENTAL EVALUATION

##### A. Electrical Testing

Electrical testing of the micro-relay consisted of dc, small-signal RF, and high-power RF characterizations. The actuation

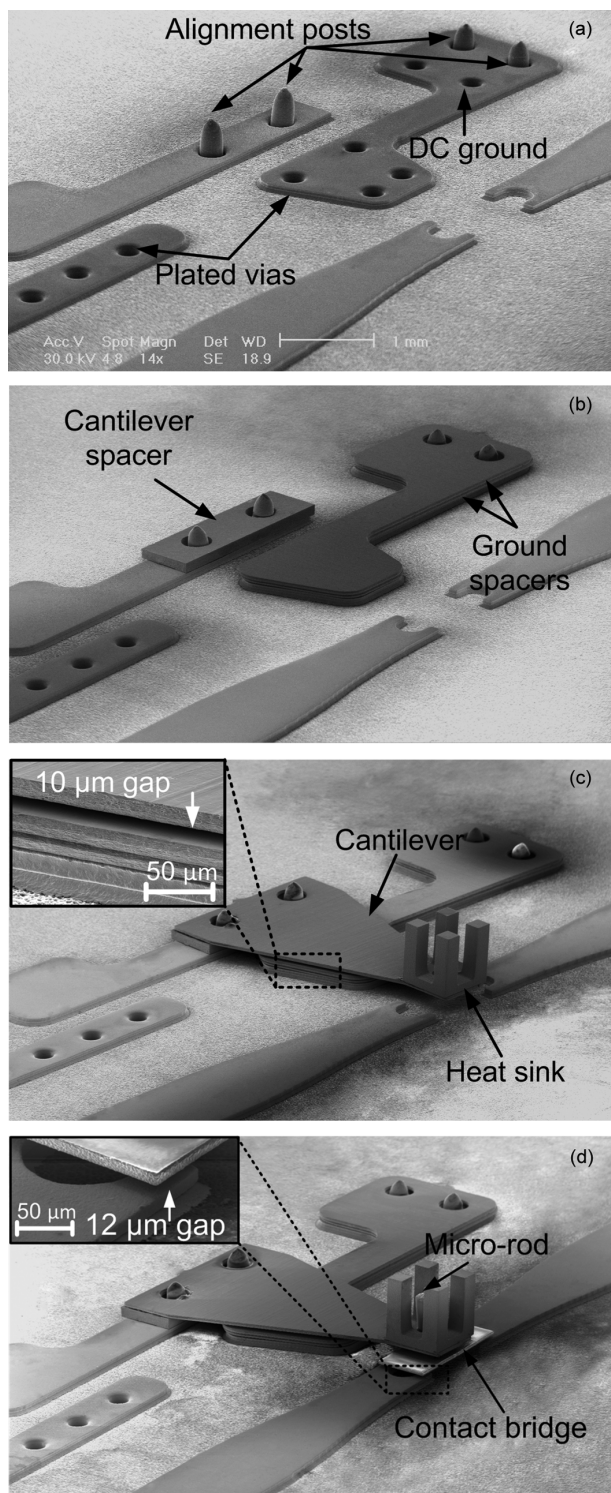


Fig. 7. Assembly sequence for the RF micro-relay. (a) Alignment posts inserted. (b) Cantilever and ground spacers (SS304) aligned on top of the posts through the perforations and anchored with electrically conductive epoxy. (c) Cantilever and the heat sink placed on top. Interelectrode gap of  $10\ \mu\text{m}$  and stacked PCB-spacer-cantilever structure are shown in the inset. (d) Contact bridge placed on the signal line and coupled with the cantilever through an embedded micro-rod fixed with epoxy in the midsection of the heat sink, ensuring uniform contact when actuated. Contact gap is shown in the inset.

concept and the test circuit for the micro-relay are shown in Fig. 8(a). The inputs are the actuation voltage ( $V_G$ ), electrical ground, and two-port RF in and RF out, which were applied on

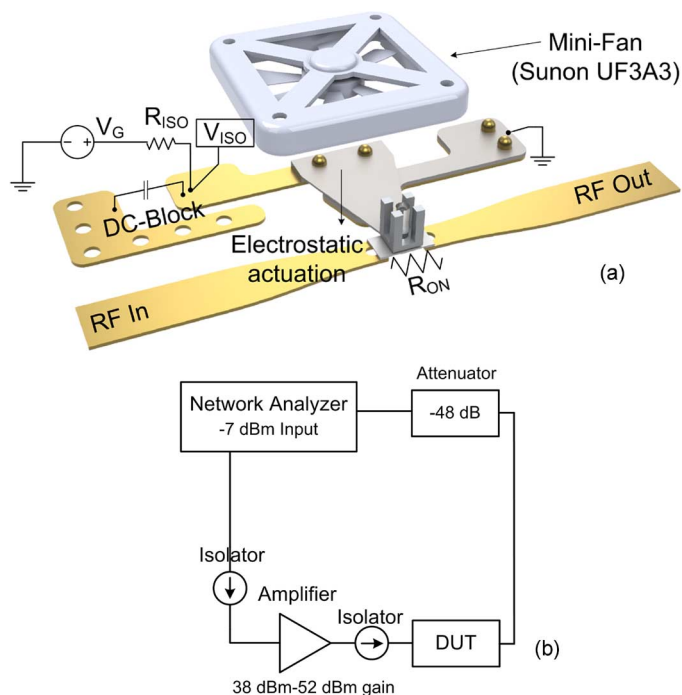


Fig. 8. (a) Circuitry for testing of three-terminal RF micro-relay. Actuation voltage  $V_G$  was used for the electrostatic actuation.  $V_{ISO}$  was monitored to detect any leakage with a  $1\text{-M}\Omega$  resistor,  $R_{ISO}$ , and was always equal to  $V_G$ .  $R_{ON}$  was the on-state resistance and included the contact resistance, bridge resistance, and parasitics. A  $1\text{-pF}$  surface mount capacitor was used for dc blocking. RF input and outputs were realized via SMA coaxial connectors. (b) High-power RF test setup (limited to  $45\ \text{dBm}$ ,  $30\ \text{W}$  of maximum RF power at  $3\ \text{GHz}$ ).

the pull-down electrode, dc ground electrode, and transmission line through SMA-type connectors, respectively. The RF signal was replaced with a line current (limited to  $10\text{-V}$  compliance) for dc ohmic-contact characterization. The cantilever isolation is monitored by voltage  $V_{ISO}$ . Under normal operation no current flow across the isolation resistor,  $R_{ISO}$  ( $1\ \text{M}\Omega$ ), is expected. Therefore,  $V_G$  and  $V_{ISO}$  are normally the same. The leakage current will cause a voltage drop across  $R_{ISO}$  if the cantilever is shorted to the dc ground electrode, and result in a  $V_{ISO}$  lower than  $V_G$ . Testing circuitry also included a  $1\text{-pF}$  dc blocking capacitor that was surface mounted between the pull-down electrode and the dc blocking electrode. All the tests were run in air ambient with unpackaged devices.

The on-state resistance of the micro-relay,  $R_{ON}$ , was characterized in dc by an  $I$ - $V$  sweep. The components of  $R_{ON}$  included contact resistance, contact bridge resistance, and the parasitics due to assembly imperfections. The pull-down voltage for the micro-relay was  $90\ \text{V}$  and the corresponding on-state resistance for tested devices was approximately  $2.5\ \Omega$ .  $R_{ON}$  was reduced to  $1.8\ \Omega$  for an actuation voltage of  $130\ \text{V}$ . Past this point,  $R_{ON}$  did not decrease significantly.

Fig. 9 shows the hysteresis in the tip displacement of the cantilever. The displacement was recorded using the laser displacement sensor. The voltage was swept from  $0$  to  $150\ \text{V}$  and back to  $0\ \text{V}$ . The pull-down voltage was around  $90\ \text{V}$ , in good agreement with the  $85\text{-V}$  design value. During the release, electrostatic force and mechanical restoring force are equal in magnitude, assuming the absence of adhesion, van der Waals adhesion

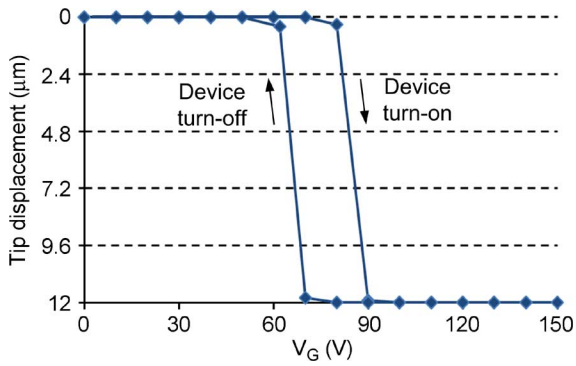


Fig. 9. Switching hysteresis. Vertical displacement at the tip of the cantilever was recorded using a laser displacement sensor with 0–150–0-V actuation voltage sweep. Device pull-down and turn-off voltages were 90 and 62 V, respectively. Device stiffness of 159 N/m was extracted.

forces, and self-actuation. The spring constant can then be extracted from the turn-off voltage of approximately 62 V using the following equation [6]:

$$F_{el} = F_k \Rightarrow k = \frac{1}{2} \frac{\varepsilon_0 W w V_{off}^2}{g^2 x}. \quad (6)$$

The mechanical spring constant was 159 N/m. This is slightly larger than the simulated value of 142 N/m, possibly due to structural assembly flaws. The electrostatic actuation and mechanical recoil forces were extracted as 4.5 and 3 mN, respectively.

Small-signal RF analysis involved experimental characterization of  $S$ -parameters, and comparison to previously performed small-signal analysis for Configuration-3. In the down-state, characteristic impedance of the contact bridge was 64  $\Omega$  [see Fig. 10(a)]. The down-state insertion loss was better than 0.2 and 0.4 dB for up to 5 and 10 GHz, respectively [see Fig. 10(b)]. In the up-state, 110-fF capacitance was extracted from the simulations [see Fig. 11(a)]. The isolation was better than 25 and 13 dB up to 5 and 10 GHz, respectively [see Fig. 11(b)]. The resonance, which occurred around 5 GHz, was mainly due to the dc-block capacitor and the inductance of the pull-down electrode. Overall, experimental data were in good agreement with results from HFSS.

The high-power testing setup is shown in Fig. 8(b). The test consisted of progressive sweeps through 11 discrete gain levels, reaching the amplifier limit of 30 W of incident RF power at 3 GHz (Amplifier Research 30W1000B). Changes in the down-state insertion loss and the up-state isolation were observed under hot-switching conditions for two on-state times: 1 and 20 s. For the down-state,  $V_G$  was maintained constant at 130 V. During the tests, heat management with upward forced cooling (0.22 m/s air flow) was used by suspending the mini-fan above the device. The effect of prolonged on-state times on  $S_{21}$  was observed. For 1-s on-state times, insertion loss in the down-state was better than 0.25 dB for up to 10 W of RF power and it increased to over 0.4 dB at around 18.5 W, where the device failed due to microwelding. The up-state isolation was approximately 26 dB over the power sweep range. Only minimal fluctuations were present and self-actuation was not observed. For 20-s on-state times, insertion loss in the

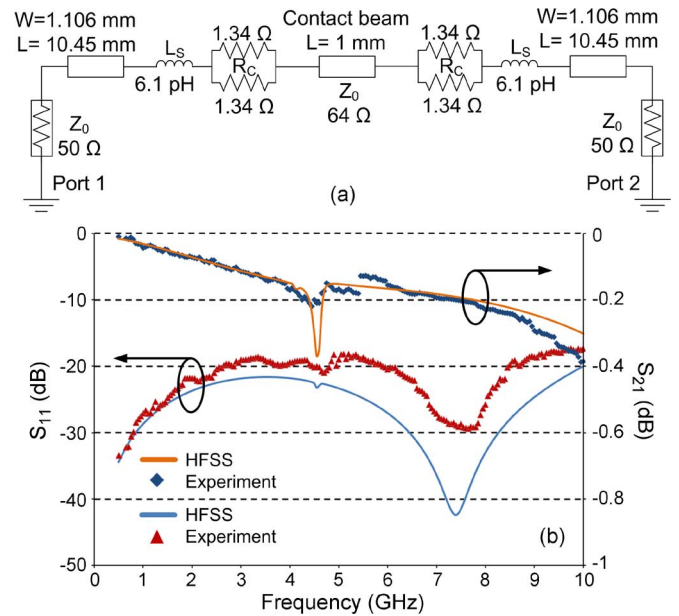


Fig. 10. (a) Equivalent circuit for the switch in the down-state. An actuation voltage of 130 V was maintained. Characteristic impedance of the contact bridge was 64  $\Omega$ . (b) Down-state small-signal analysis for 500 MHz–10 GHz. Experimental data compared with HFSS. The down-state insertion loss was below 0.2 dB for up to 5 GHz.

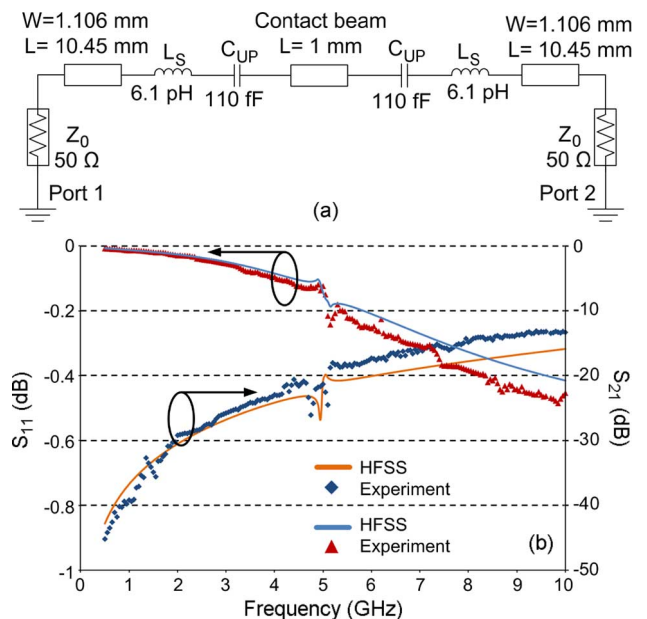


Fig. 11. (a) Equivalent circuit for the switch in the up-state. Up-state capacitance of 110 fF was extracted from the full-wave simulations. (b) Up-state small-signal analysis for 500 MHz–10 GHz. Experimental data compared with HFSS. The isolation was better than 25 dB up to 5 GHz.

down-state degraded noticeably faster to near 0.4 dB at 7 W at which point the device failed. Similarly, isolation remained around 26 dB for up to 30 W and no self-actuation was observed (Fig. 12).

### B. Thermal Testing

The characterization of the micro-relay contact temperatures was performed with 1- and 20-s on-state times under the forced air cooling conditions. A preliminary assessment of the thermal

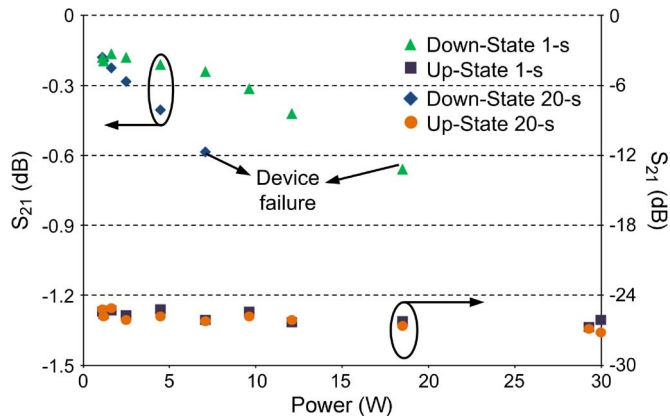


Fig. 12. High-power testing for the RF micro-relay. Tests were performed at 3 GHz and at power levels progressively reaching 30 W, at 130-V actuation voltage and in air ambient. Heat management was used throughout the testing with upward forced cooling (compatible with Sunon UF3A3 mini fan,  $10 \times 10 \times 3 \text{ mm}^3$  size, 0.22 m/s air flow). For 1-s on-state times, insertion loss in the down-state was below 0.25 dB for up to 10 W and increased to over 0.4 dB at around 18.5 W where the device failure occurred due to micro-welding. The up-state isolation was around 26 dB throughout and self-actuation was not observed. For 20-s on-state times, the down-state insertion loss increased significantly faster to approximately over 0.4 dB at 7 W where microwelding occurred. In the up-state, isolation was around 26 dB up to 30 W and no failures were observed.

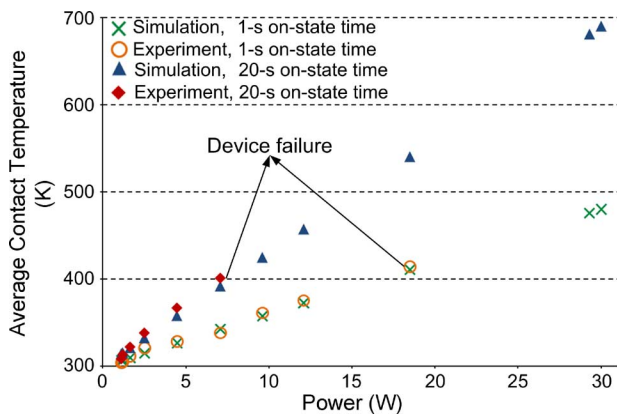


Fig. 13. Average contact temperature for 1- and 20-s on-state times in air ambient with the forced cooling. Contact temperatures were measured using an infrared thermometer. Experimental data was compared with the thermal model. The device with 1- and 20-s on-state times failed at 18.5 and 7 W, respectively.

conditions was done by measuring the contact temperature at the end of each 1- and 20-s actuation time periods during which varying levels of RF power were maintained. The thermal and high-power testing described previously were carried out simultaneously on the same devices. The measurements were performed using an infrared thermometer (Optris LaserSight, 1-mm laser diameter). The ambient temperature was 300 K. The laser was directed at the contact regions and average contact temperature was measured at the end of each actuation cycle. The experimental results were compared with the thermal model.

Fig. 13 shows the average contact temperatures. Failures associated with micro-welding at 18.5 and 7 W occurred past 400 K for devices with 1- and 20-s on-state times, respectively. The experimental results and the thermal model overall agreed well.

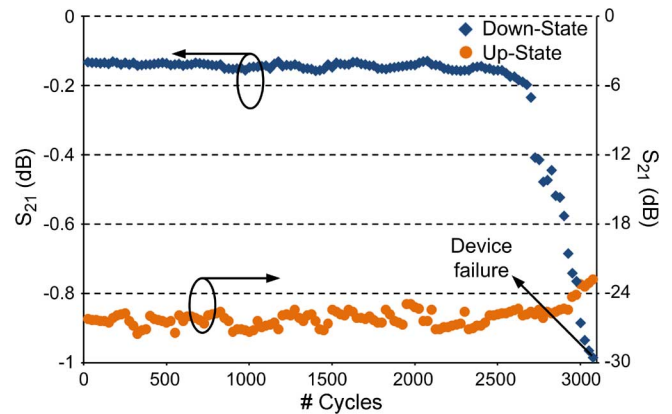


Fig. 14. Lifetime characterization of the micro-relay. The test was run under the hot switching conditions in air ambient with forced air cooling. Test conditions included 1 W of RF power at 3 GHz and 130-V actuation voltage. The switching frequency was 0.5 Hz and duty cycle was 50%. A drastic increase in the down-state insertion loss was observed past 2800 cycles leading to failure in the 3074th cycle at nearly 1 dB. Isolation was reduced slightly to 22.5 dB at the point of failure.

### C. Lifetime Testing

The lifetime characterization of the micro-relay was realized under the hot switching conditions. Continuous RF power of 1 W was applied at 3 GHz. The micro-relay was operated at 0.5-Hz frequency with 50% duty cycle following 1-s on-state times. Actuation voltage,  $V_G$  was maintained at 130 V during the on-state. The test was carried out in air ambient with forced cooling.  $S_{21}$  for both the up- and down-state was recorded up to the point of device failure. The down-state insertion loss was near constant below 0.2 dB and increased notably past 2800 cycles (Fig. 14). The device failure occurred in the down-state at the 3074th cycle with 1-dB insertion loss. The up-state isolation was degraded slightly from 26 dB and it was recorded 22.5 dB at the point of failure.

## V. DISCUSSION AND CONCLUSIONS

Electrostatically actuated micro-relays with Pt-Rh contacts were directly assembled on a PCB iteratively optimized for RF performance. Unpackaged test structures with 6.4-mm<sup>2</sup> footprints and 90-V pull-down voltage, were tested for small-signal performance and high power-handling capability in an air ambient. For small signal, the down-state insertion loss and the up-state isolation were better than 0.2 and 25 dB up to 5 GHz, respectively. Experimental data were in good agreement with results from HFSS. High-power testing was performed for up to 30 W at 3 GHz for both 1- and 20-s on-state times. Heat management was employed through forced air cooling using a commercially available mini-fan placed above the devices. Elongated on-state times lead to an early device failure. Micro-welding occurred in the down-state at 18.5 and 7 W for 1- and 20-s on-state times, respectively. No self-actuation was observed in the up-state. It is envisioned that shorter on-state times can potentially provide higher peak power handling.

The lifetime of an unpackaged micro-relay operating in air was 3074 cycles under the hot switching conditions of 1-W RF power. One of the potential contributors degrading device lifetime is the frictional polymerization, which is known to be

caused by the wipe and pure normal contact between Pt group contact metals [28]. Device packaging is essential to potentially eliminate this phenomenon and to elongate the device lifetime.

The test structures evaluated in this study were comparable in size with the packaged RF microelectromechanical systems (MEMS) devices. The power handling was from  $4\times$  to  $5\times$  higher than that reported for other RF MEMS relays of similar size [16], [29], and [30]. Conversely, on-state resistances were relatively high.

The main goal of this effort has been to investigate the RF power-handling limits of micro-relays with bulk foil contact elements. Based on the performance of the RF micro-relays described in this study, the use of chemically inert and mechanically robust bulk foil alloys such as Pt–Rh appears promising for high-power applications. Future efforts may include the batch-mode mass production of the structure, and the device packaging.

## REFERENCES

- [1] S. Lucyszyn, "Review of radio frequency microelectromechanical systems technology," in *Proc. IEEE Sci., Meas. Technol.*, 2004, vol. 151, no. 2, pp. 93–103.
- [2] H. J. Santos, G. Fischer, H. A. C. Tilmans, and J. T. M. Beek, "RF MEMS for ubiquitous wireless connectivity," *IEEE Microw. Mag.*, vol. 5, no. 4, pp. 36–49, 2004.
- [3] J. Costa, T. Ivanov, J. Hammond, J. Gering, E. Glass, J. Jorgenson, D. Dening, D. Kerr, J. Reed, S. Crist, T. Mercier, S. Kim, and P. Gorisse, "Integrated MEMS switch technology on SOI-CMOS," in *Proc. Solid-State Sens., Actuators, Microsyst. Workshop*, Hilton Head, SC, 2008, pp. 18–21.
- [4] H.-S. Lee, C. H. Leung, J. Shi, S.-C. Chang, S. Lorincz, and I. Nedelcsu, "Integrated microrelays: Concept and initial results," *J. Microelectromech. Syst.*, vol. 11, no. 2, pp. 147–153, Apr. 2002.
- [5] R. Robin, O. Millet, K. Segueni, and L. Buchaillet, "Low actuation voltage SPDT RF-MEMS  $K$ -band switch using a single gold membrane," in *Proc. 19th IEEE Int. Microelectromech. Syst. Conf.*, 2009, pp. 872–875.
- [6] G. M. Rebeiz, *RF MEMS: Theory, Design and Technology*. Hoboken, NJ: Wiley, 2003.
- [7] P. D. Grant and M. W. Denhoff, "A Comparison between RF switches and semiconductor switches," in *Proc. IEEE Int. MEMS, Nano, Smart Syst. Conf.*, 2004, pp. 515–521.
- [8] R. Chan, R. Lesnick, D. Becher, and M. Feng, "Low-actuation voltage RF MEMS shunt switch with cold switching lifetime of seven billion cycles," *J. Microelectromech. Syst.*, vol. 12, no. 5, pp. 713–719, Oct. 2003.
- [9] H. S. Newman, J. L. Ebel, D. Judy, and J. Maciel, "Lifetime measurements on a high-reliability RF-MEMS contact switch," *IEEE Microw. Wireless Compon. Lett.*, vol. 18, no. 2, pp. 100–102, Feb. 2008.
- [10] A. Fruehling, R. Pimpinella, R. Nordin, and D. Peroulis, "A single crystal silicon DC–40 GHz RF MEMS switch," in *IEEE MTT-S Int. Microw. Symp. Dig.*, 2009, pp. 1633–1636.
- [11] C. D. Patel and G. M. Rebeiz, "RF MEMS metal-contact switches with mN-contact and restoring forces and low process sensibility," *IEEE Trans. Microw. Theory Tech.*, vol. 59, no. 5, pp. 1230–1237, May 2011.
- [12] B. Norvell, R. Hancock, J. Smith, M. Pugh, S. Theis, and J. Kvitek, "Micro electro mechanical switch (MEMS) technology applied to electronically scanned arrays for space based radar," in *Proc. IEEE Aerosp. Conf.*, 1999, vol. 3, pp. 239–247.
- [13] K. Van Caekenbergh, "RF MEMS on the radar," *IEEE Microw. Mag.*, vol. 10, no. 6, pp. 99–116, 2009.
- [14] H. Kwon, D.-J. Choi, J.-H. Park, H.-C. Lee, Y.-H. Park, Y.-D. Kim, H.-J. Nam, Y.-C. Joo, and J.-U. Bu, "Contact materials and reliability for high power RF-MEMS switches," in *Proc. 20th IEEE Int. Microelectromech. Syst. Conf.*, 2007, pp. 231–234.
- [15] B. D. Jensen, L. L. W. Chow, K. Huang, K. Saitou, J. L. Volakis, and K. Kurabayashi, "Effect of nanoscale heating on electrical transport in RF MEMS switch contacts," *J. Microelectromech. Syst.*, vol. 14, no. 5, pp. 935–946, 2005.

- [16] R. A. Coutu, P. E. Kladitis, K. D. Leedy, and R. L. Crane, "Selecting metal alloy electric contact materials for MEMS switches," *J. Microelectromech. Microeng.*, vol. 14, pp. 1157–1164, 2004.
- [17] N. E. McGruer, G. G. Adams, L. Chen, Z. J. Guo, and Y. Du, "Mechanical, thermal, and material influences on ohmic-contact-type MEMS switch operation," in *Proc. 19th IEEE Int. Microelectromech. Syst. Conf.*, 2006, pp. 230–233.
- [18] B. Fischer, A. Behrends, D. Freund, D. F. Lupton, and J. Merker, "High temperature mechanical properties of the platinum group metals," *Platinum Metals Rev.*, vol. 43, no. 1, pp. 18–28, 1999.
- [19] G. Dereli, T. Cagin, M. Uludogan, and M. Tomak, "Thermal and mechanical properties of Pt–Rh alloys," *Philosoph. Mag. Lett.*, vol. 75, pp. 209–217, 1997.
- [20] S. Duffy, C. Bozler, S. Rabe, J. Knecht, L. Travis, P. Wyatt, C. Keast, and M. Couker, "MEMS microswitches for reconfigurable microwaves circuitry," *IEEE Microw. Wireless Compon. Lett.*, vol. 11, no. 3, pp. 106–108, Mar. 2001.
- [21] S. Majumder, J. Lampen, R. Morrison, and J. Maciel, "A packaged, high-lifetime ohmic MEMS RF switch," in *IEEE MTT-S Int. Microw. Symp. Dig.*, 2003, vol. 3, pp. 1935–1938.
- [22] F. M. Ozkeskin, S. Choi, K. Sarabandi, and Y. B. Gianchandani, "Metal foil RF micro-relay with integrated heat sink for high power applications," in *Proc. 24th IEEE Int. Microelectromech. Syst. Conf.*, 2011, pp. 776–779.
- [23] S. Cimentalay and R. E. Fulton, "Parameter design of heat sink: Multiple trade-offs," in *Proc. ASME Annu. Winter Meeting*, 1994, vol. EEP-9, pp. 53–59.
- [24] R. Holm, *Electric Contacts*. Berlin, Germany: Springer-Verlag, 1968.
- [25] P. G. Slade, Ed., *Electrical Contacts: Principles and Applications*. New York: Marcel Dekker, 1999.
- [26] F. P. Bowden and D. Tabor, *Friction and Lubrication of Solids*. Oxford, U.K.: Oxford Univ. Press, 1964, vol. 2.
- [27] K. Takahata and Y. B. Gianchandani, "Batch mode micro-electro-discharge machining," *J. Microelectromech. Syst.*, vol. 11, no. 2, pp. 102–110, Apr. 2002.
- [28] W. H. Abbott and W. K. Campbell, "Frictional polymer formation on precious metals. Experimental observation," in *Proc. 9th Int. Elect. Contact Phenomena Conf.*, Chicago, IL, 1978, pp. 359–363.
- [29] E. S. Shim, W. Choi, Y. Kim, Y. Kwon, J. S. No, S. Nam, and D.-I. Cho, "Hot-switching test of non-contact type MEMS switch," in *IEEE MTT-S Int. Microw. Symp. Dig.*, 2007, pp. 1809–1812.
- [30] A. Stehle, C. Siegel, V. Ziegler, B. Schoenlinner, U. Prechtel, H. Seidel, and U. Schmid, "High-power handling capability of a low complexity RF-MEMS switch in  $K$ -band," *IEEE Microw. Electron. Lett.*, vol. 43, no. 24, pp. 1367–1368, 2007.



turing.

**Fatih M. Ozkeskin** (S'11–M'12) received the B.S. degree in mechatronics engineering from Sabanci University, Istanbul, Turkey, in 2006, the M.S. degree in mechanical engineering from Texas A&M University, College Station, in 2008, and the M.S. degree in electrical engineering and Ph.D. degree in mechanical engineering from The University of Michigan at Ann Arbor, both in 2011.

He is currently a Process Engineer with Applied Materials, Santa Clara, CA. His research interests include MEMS devices and micro/nano manufac-



**Sangjo Choi** (S'09) received the B.S. degree in electrical engineering from The University of Texas at Dallas, in 2008, the M.S. degree in electrical engineering from The University of Michigan at Ann Arbor, in 2010, and is currently working toward the Ph.D. degree in applied electromagnetics at The University of Michigan at Ann Arbor.

He is currently a Graduate Research Assistant with the Radiation Laboratory, The University of Michigan at Ann Arbor.



**Kamal Sarabandi** (S'87–M'90–SM'92–F'00) received the B.S. degree in electrical engineering from the Sharif University of Technology, Tehran, Iran, in 1980, and the M.S. degree in electrical engineering, M.S. degree in mathematics, and Ph.D. degree in electrical engineering from The University of Michigan at Ann Arbor in 1986, 1989, and 1989, respectively.

He is currently the Director of the Radiation Laboratory, and the Rufus S. Teesdale Professor of Engineering with the Department of Electrical Engineering and Computer Science, The University of Michigan at Ann Arbor. He possesses 25 years of experience with wave propagation in random media, communication channel modeling, microwave sensors, and radar systems and leads a large research group including two research scientists and 14 Ph.D. students. He has graduated 37 Ph.D. candidates and supervised numerous post-doctoral students. He has served as the Principal Investigator on many projects sponsored by the National Aeronautics and Space Administration (NASA), Jet Propulsion Laboratory (JPL), Army Research Office (ARO), Office of Naval Research (ONR), Army Research Laboratory (ARL), National Science Foundation (NSF), Defense Advanced Research Projects Agency (DARPA), and a large number of industries. He currently leads the Center for Microelectronics and Sensors, funded by the Army Research Laboratory under the Micro-Autonomous Systems and Technology (MAST) Collaborative Technology Alliance (CTA) Program. He has authored or coauthored many book chapters and over 180 papers in refereed journals on miniaturized and on-chip antennas, metamaterials, electromagnetic scattering, wireless channel modeling, random media modeling, microwave measurement techniques, radar calibration, inverse scattering problems, and microwave sensors. He has also had over 420 papers and invited presentations in many national and international conferences and symposia on similar subjects. His research interests include microwave and millimeter-wave radar remote sensing, metamaterials, electromagnetic wave propagation, and antenna miniaturization.

Dr. Sarabandi was a member of the National Aeronautics and Space Administration (NASA) Advisory Council appointed by the NASA Administrator in two consecutive terms from 2006 to 2010. He is a vice president of the IEEE Geoscience and Remote Sensing Society (GRSS). He is a member of the Editorial Board of the PROCEEDINGS OF THE IEEE. He was an associate editor of the IEEE TRANSACTIONS ON ANTENNAS AND PROPAGATION and the IEEE SENSORS JOURNAL. He is a member of Commissions F and D, URSI. He is listed in *American Men and Women of Science*, *Who's Who in America*, and *Who's Who in Science and Engineering*. He was the recipient of the Henry Russel Award of the Regent of The University of Michigan at Ann Arbor, the

1999 GAAC Distinguished Lecturer Award of the German Federal Ministry for Education, Science, and Technology, the 1996 Electrical Engineering and Computer Science (EECS) Department Teaching Excellence Award, a 2004 College of Engineering Research Excellence Award, the 2005 IEEE GRSS Distinguished Achievement Award, The University of Michigan at Ann Arbor Faculty Recognition Award, the 2006 Best Paper Award of the Army Science Conference, the 2008 Humboldt Research Award of the Alexander von Humboldt Foundation of Germany, the Best Paper Award of the IEEE Geoscience and Remote Sensing Symposium, and the 2010 Distinguished Faculty Achievement Award of The University of Michigan at Ann Arbor. The IEEE Board of Directors announced him as the recipient of the 2011 IEEE Judith A. Resnik Medal. In the past several years, joint papers presented by his students at a number of international symposia (IEEE APS'95,'97,'00,'01,'03,'05,'06,'07; IEEE IGARSS'99,'02,'07,'11; IEEE IMS'01, USNC URSI'04,'05,'06,'10, and AMTA'06, URSI GA 2008) have received Best Paper Awards.



**Yogesh B. Gianchandani** (S'86–M'86–SM'05–F'10) received the B.S. degree from the University of California at Irvine, in 1984, the M.S. degree from the University of California at Los Angeles (UCLA), in 1986, and the Ph.D. degree from The University of Michigan at Ann Arbor, in 1994, all in electrical engineering.

He is currently a Professor with The University of Michigan at Ann Arbor, with a primary appointment with the Electrical Engineering and Computer Science Department and a courtesy appointment with

the Mechanical Engineering Department. He also serves as the Director for the Center for Wireless Integrated MicroSensing and Systems (WIMS<sup>2</sup>). From 2007 to 2009, he was also the Program Director for Micro and Nano Systems within the Electrical, Communication, and Cyber Systems Division (ECCS), National Science Foundation (NSF). He has authored or coauthored over 250 papers in journals and conferences. He holds approximately 35 U.S. patents (issued or pending). He was a Chief Co-Editor of *Comprehensive Microsystems: Fundamentals, Technology, and Applications* (Elsevier, 2008). His research interests include all aspects of design, fabrication, and packaging of micromachined sensors and actuators and their interface circuits.

Dr. Gianchandani has been an editor or a member of the Editorial Board of several journals. He was a general co-chair for the 2002 IEEE/ASME International Conference on MEMS.